Paleoceanography and Paleoclimatology

RESEARCH ARTICLE
10.1029/2020PA003979

Reconstructing Depositional Rates and Their Effect on Paleoenvironmental Proxies: The Case of the Lau Carbon Isotope Excursion in Gotland, Sweden

E. Jarochowska[1], T. Nohl[1], M. Grohganz[1], N. Hohmann[1], T. R. A. Vandenbroucke[2], and A. Munnecke[1]

[1]GeoZentrum Nordbayern, Fachgruppe Paläoumwelt, Friedrich-Alexander-Universität Erlangen-Nürnberg, Erlangen, Germany, [2]Department of Geology, Ghent University, Ghent, Belgium

Key Points:

- Relative age models are reconstructed from concentrations of Th, carbonate, and pelagic palynomorphs
- $\delta^{13}C_{carb}$ and elemental proxies for redox conditions are transformed using the age models
- Accounting for depositional rates can decrease peaks in redox proxies by up to 45% and make the $\delta^{13}C_{carb}$ excursion appear more abrupt

Correspondence to:
E. Jarochowska,
emilia.jarochowska@fau.de

Citation:
Jarochowska, E., Nohl, T., Grohganz, M., Hohmann, N., Vandenbroucke, T. R. A., & Munnecke, A. (2020). Reconstructing depositional rates and their effect on paleoenvironmental proxies: The case of the Lau Carbon Isotope Excursion in Gotland, Sweden. *Paleoceanography and Paleoclimatology*, *35*, e2020PA003979. https://doi.org/10.1029/2020PA003979

Received 13 MAY 2020
Accepted 5 DEC 2020

Abstract Variations in depositional rates affect the temporal depositional resolutions of proxies used for paleoenvironmental reconstructions; for example, condensation can make reconstructed environmental changes appear very abrupt. This is commonly addressed by transforming proxy data using age models, but this approach is limited to situations where numerical ages are available or can be reliably inferred by correlation. Here we propose a new solution, in which relative age models are constructed based on proxies for depositional rates. As a case study, we use the onset of the late Silurian Lau Carbon Isotope Excursion (LCIE) in Gotland, Sweden. The studied succession is a gradual record of shallowing upward in a tropical, neritic carbonate platform. As proxies for depositional rates we tested thorium concentration, carbonate content, and the concentration of pelagic palynomorphs. These three proxies were used to create relative age models using the previously published DAIME model. We applied these models to transform the $\delta^{13}C_{carb}$ values as well as concentrations of selected redox-sensitive elements. The three relative age models yielded qualitatively similar results. In our case study, variations in depositional rates resulted in peaks of redox proxies appearing up to 76% higher when taken at face value, compared to when accounting for these rates. In the most extreme cases, our corrections resulted in a reversal in the stratigraphic trend of elemental concentrations. This approach can be applied and developed across depositional setting and types of paleoenvironmental proxies. It provides a flexible tool for developing quantitative models to improve our understanding of the stratigraphic record.

Plain Language Summary The depositional rate reflects how quickly a given thickness of sedimentary rock forms. Abrupt changes in environmental signals recorded in an interval of strata can be the result of (1) fast changes in environmental conditions and average sedimentation rate or (2) average changes in environmental conditions and slow sedimentation rate. To correct for this effect, age models are used, but they are often not available or lack sufficient resolution to detect rapid changes in the environment. We propose a method to estimate relative changes in depositional rates and test it in a sedimentary section on the Swedish island of Gotland. The section preserves geochemical records of a carbon cycle perturbation, expressed as shifts in carbon isotopes. It has also been proposed to record periods of oxygen depletion in marine water, detectable as enrichment in elements sensitive to redox conditions. We measured these parameters and compared the original values as preserved in the section with values corrected for depositional rates. We show that (1) perturbations of the carbon cycle were most likely more rapid than they appear in the section and (2) high depositional rates during the carbon cycle perturbation partly disguised the intervals of oxygen depletion.

1. Introduction

1.1. How Paleoenvironmental Information in Sedimentary Rocks Is Transformed by Depositional Rates

Variations in the volume and rate of influx of sediment can completely transform fossil accumulations by concentrating and diluting individual hard parts. In extreme cases, they can lead to mixing of fossils from completely different environments and stratigraphic ages at condensed surfaces or to smearing out of the record of geologically abrupt events (Carroll et al., 2016; Fürsich & Aberhan, 1990; Kidwell, 1998; Kowalewski, 1996). Less dramatic variations lead to records that are altered in more obscure manner,

though these may be as important to understand. Simple models varying the input of sediment and skeletal hard parts allow us to simulate the entire range of outcomes, where, for example, a barren interval or a bloom horizon might be obtained by increasing or decreasing the depositional rate (Dominici et al., 2018; Kidwell, 1985). In shallow aquatic and terrestrial settings, changes in the ecosystem and the environment happen faster than the resolution of the depositional system and virtually all biological information preserved is shredded to some degree (Jerolmack & Paola, 2010; Kowalewski & Bambach, 2008; Straub et al., 2020). Individual events can be distinguished in the geological record only if they take place at a temporal scale lower or equal to that of the depositional resolution of the given succession. Although this has been addressed in various ways when analyzing the fossil record (Tomašových et al., 2017; Tomašových & Kidwell, 2010), individual sediment particles are, principally, subject to the same processes, for example, reworking of sand grains by water or burrowing organisms and dilution or condensation by surrounding sediment. Therefore, any parameters measured in these particles will be affected by the processes that are already well known to alter the fossil record. This includes geochemical measurements such as isotope ratios in bulk-rock carbonates or trace element composition. The record of changes in any environment derived from proxies based on geochemistry needs to account for the stratigraphic completeness and depositional resolution of the sediment in which they are measured.

The depositional resolution, that is, the smallest duration that can be distinguished in a sedimentary deposit, is estimated to be typically around 10^2–10^4 years in bedded nearshore and shelfal deposits (Kowalewski & Bambach, 2008). The depositional resolution is the product of processes including depositional rates (i.e., the outcome of net sedimentation and erosion), bioturbation, and mechanical and chemical destruction of specific fractions, for example, decay of organic matter, boring and dissolving of bioclasts, winnowing, and selective cementation. In this study, we investigate the impact of depositional rates on how changes in the chemical composition of the sediment are preserved and interpreted. These rates are generally calculated in sections where some numerical ages are available and several statistical approaches are available for radiocarbon-dated sections (Parnell et al., 2011). But such ages are not available for many sections at all—particularly in deep time—and are too scattered across the geological record to allow for high-resolution age models for any given paleoenvironmental change. On the other hand, sedimentary and sequence-stratigraphic indicators often provide insights into relative changes in the depositional rate at high resolution, for example, flooding surfaces at parasequence bases or firmgrounds. Changes in depositional rates within a given basin or facies model are often highly predictable and vary systematically together with the position within the depositional sequence (Brett, 1995; Holland, 2000; Jarochowska et al., 2018; Ray & Thomas, 2007).

1.2. The Late Silurian Lau Carbon Isotope Excursion

Here we investigate how changing depositional rates can alter the chemical composition and common elemental redox proxies in a Silurian carbonate section. As a case study, we use the onset of the Lau Carbon Isotope Excursion (LCIE), the strongest positive $\delta^{13}C$ excursion in the Phanerozoic (Jux & Steuber, 1992; Munnecke et al., 2010; Samtleben et al., 1996; Wenzel & Joachimski, 1996; Wigforss-Lange, 1999). This excursion is associated with global rapid sea level changes (Antoshkina, 2018; Chadimová et al., 2015; Eriksson & Calner, 2008; Kozłowski & Sobień, 2012; Loydell & Frýda, 2011; McLaughlin et al., 2019; Munnecke et al., 2010), resulting in a potential strong imprint of facies and changing depositional rate on the record of carbon isotopes and associated changes in biota and seawater chemistry (Jarochowska & Kozłowski, 2014; Mergl et al., 2018). Globally, the duration of the entire LCIE is indirectly constrained to have lasted from ca. 422.96 ± 2.28 to 424.96 ± 1.15 Ma (Gradstein et al., 2012), but the onset is estimated to have been very rapid. The global sea level fall synchronous with the onset of the regression is postulated to have been glacioeustatically driven, supporting its short duration (Sproson, 2020). The duration of the onset of the excursion (the rise from background to peak values), examined here, is below the resolution of Silurian biostratigraphy as it was shorter than one conodont biochron (of the *Polygnathoides siluricus* Biozone), and in most sections the rising values are constrained to one graptolite zone (*Neocucullograptus kozlowskii*; Jeppsson, 2005).

The onset of the LCIE and other high-amplitude Silurian carbon isotope excursions have been postulated to systematically coincide with changes in seawater chemistry, including increased stratification of the water column and anoxia (Bowman et al., 2019; Cramer & Saltzman, 2007; Hammarlund et al., 2019;

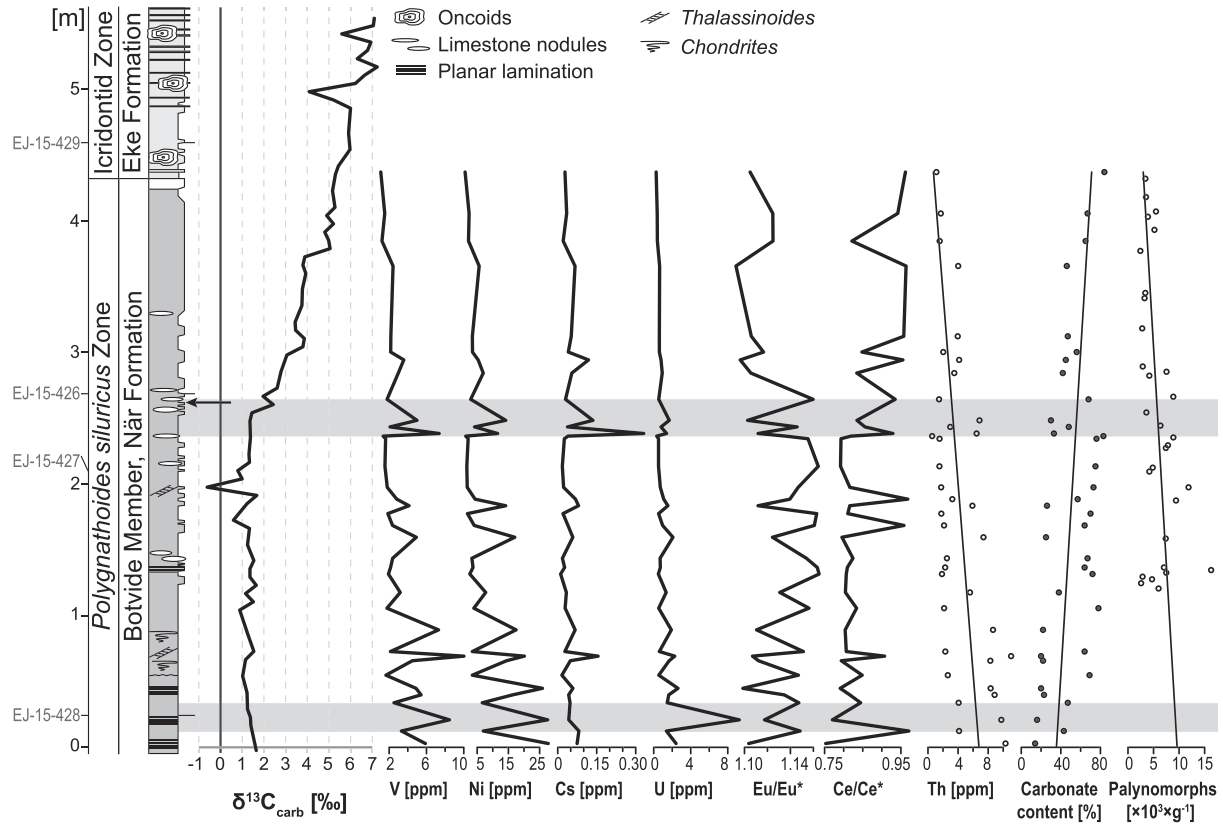

Figure 1. Lithological log of the Bodudd 1 section, Gotland, Sweden, changes of the $\delta^{13}C_{carb}$ values, selected redox-sensitive proxies in the carbonate fraction, variables used as proxies for relative age models, and positions of thin-section samples (EJ_15-xxx) shown in Figure 2. All data are newly produced in this study except for palynomorph concentration, which is from Stricanne et al. (2006). Gray bars highlight peaks discussed in the text, and the arrow marks the position of the boundary between the När and Eke formations according to Jeppsson et al. (2007).

McLaughlin et al., 2012; Munnecke et al., 2012; Smolarek et al., 2016; Sullivan et al., 2018; Vandenbroucke et al., 2013, 2015; Vecoli et al., 2009; Young et al., 2020) manifested in enrichment of redox-sensitive proxies. What is more, these anoxic intervals have been proposed to be related with mobilization of heavy metals, which would have affected the biota (Emsbo, 2017; Munnecke et al., 2012; Vandenbroucke et al., 2015). The interpretation of these proxies and quantification of the spread and magnitude of anoxic conditions are, however, complicated by the fact that they are recorded in an interval of rapid regression, which in shallow settings is characteristically associated with facies shifts and numerous diastems. Therefore, the dynamics of element concentrations are distorted by changes in the depositional rates, creating, for example, accumulations at condensation surfaces. To circumvent these difficulties, we evaluate these proxies at a section representing the distal shelf environment of a Silurian tropical carbonate platform, at Bodudd, Gotland (Sweden) (Eriksson & Calner, 2008; Jeppsson et al., 2007; Samtleben et al., 2000). This section records a comparably continuous record of the onset of the LCIE preserved in homogenous facies (Figure 1). In such a section, it is possible to identify basic sedimentological and paleontological proxies for the depositional rate and use these to develop relative age models. Here we examine the dynamics of redox-sensitive elements and their ratios across the onset of the LCIE and account for the effects of depositional rates by transforming the original records using three relative age models. The models are based on thorium input, carbonate content, and density of pelagic palynomorphs. The age models and transformation are performed using the method introduced by Hohmann (2018).

The aim of this study is to test whether stratigraphic patterns of element concentrations, particularly of redox-sensitive trace elements, are affected by changing depositional rates and to what extent can this alter their interpretations. As a case study to perform this test, we evaluate the hypothesis that peaks in the concentration of selected elements at the onset of the LCIE at Bodudd 1 are created by sedimentary

condensation. We also propose how relative age models can be created for a given depositional setting in the absence of absolute ages and how they can be used to account for depositional rates in interpretations of data preserved in sedimentary successions.

1.3. Estimating Relative Depositional Rates

The section used here as a case study represents a common case where no absolute ages are available to create an age model. Nonetheless, for a given basin type and facies model, relative changes in depositional rates can be estimated and are often manifest in the field, for example, as flooding surfaces. A quantitative estimate of the relative depositional rate can be obtained from the inversed proportion of sediment components which are diluted by sediment input. Here we will test three relative age models based on three commonly used proxies for depositional rates. The proxies proposed here apply to carbonate platforms and can be readily measured in the absence of absolute ages: thorium concentration, the carbonate content of bulk rock, and the concentration of pelagic palynomorphs.

1.3.1. Thorium Concentration

The dynamics of both thorium and uranium in sedimentary rocks is very well understood as the concentrations of these two elements are routinely measured in spectral gamma ray logs. Among thorium isotopes, two have half-lives long enough to be relevant for sedimentology: the long-lived ^{232}Th isotope (half-life = 1.4×10^{10} years) and the short-lived ^{230}Th (half-life = 75×10^{3} years) (Bacon & Anderson, 1982). Both forms are present across conditions encountered in seawater as Th (IV), which has very low solubility and is mostly transported by adsorption (Nozaki et al., 1987). ^{230}Th in marine sediments and biogenic carbonates is largely derived from the decay of uranium, which is more soluble and therefore incorporated into calcite and aragonite crystal lattice in higher proportions. Its short half-life means, however, that in Silurian carbonates ^{230}Th will have decayed into its daughter isotopes, ^{226}Ra, ^{206}Hg, and ^{24}Ne, virtually completely. The dominant form, ^{232}Th, is transported in heavy minerals, such as zircon and monazite, and therefore accumulated in fine-grained aluminosilicate-rich siliciclastic facies (Ehrenberg & Svånå, 2001). Despite its low solubility, a small proportion of weathering-derived ^{232}Th is mobilized in seawater and incorporated in the crystal lattice of carbonate minerals (Robinson et al., 2004; Shen et al., 2008). Otherwise chemically similar, uranium differs from thorium in that uranium forms a soluble uranyl form under oxidizing conditions and is thus used as a redox proxy. The ratio Th/U is often employed as an indicator of terrigenous or marine influence (Doveton, 1994) and redox conditions in the depositional environment (Adams & Weaver, 1958). Here we use Th (effectively meaning ^{232}Th) concentration instead of the more popular Th/U ratio to avoid circularity: the relative age model based on Th content is used to evaluate the accumulation of redox-sensitive metals and test hypotheses on their precipitation due to changing redox conditions. Consequently, the relative age model cannot be based on a redox-sensitive element. Thorium concentration in carbonate and other chemically precipitated sedimentary rocks shows good correlation with total insoluble residue and can therefore be used as a proxy for the rate of carbonate deposition (Adams & Weaver, 1958).

In siliciclastic settings, Th concentration is proportional to the amount of detrital siliciclastic material forming the sediment and is therefore decreasing basinward (Adams & Weaver, 1958). In a tropical carbonate platform environment, however, Th is diluted by carbonate. Based on this, we assume Th concentration to be negatively correlated with the depositional rate in this setting. Following this assumption, the shallow, euphotic zone of most intensive carbonate production is expected to have the lowest Th concentrations, which increase with the distance from the center of the carbonate factory, that is, toward platform margin.

1.3.2. Carbonate Content

The locus of carbonate production and accumulation has shifted since the Paleozoic from the neritic factory to the pelagic realm as a result of the evolution of calcareous plankton (Ridgwell, 2005). Therefore, in post-Paleozoic oceans carbonate content cannot be used as an indicator of the proximity of the neritic carbonate platform. In the early Phanerozoic, however, carbonate content correlates well with the position along the onshore-offshore gradient and, thus, with the intensity of carbonate production (Schlager, 2003). The Baltic Basin, where the Bodudd section is located, is representative of other Paleozoic tropical-subtropical basins in terms of facies distribution (Calner et al., 2006; Lazauskienė et al., 2003; Tomczykowa, 1988). The epicratonic basin margin is formed by reefal, bioclastic, and microbial limestones, and the only clastic lithosomes are associated with forced regressive strata (Calner et al., 2006; Eriksson & Calner, 2008;

Jarochowska & Kozłowski, 2014; Kozłowski & Sobień, 2012; Radkovets, 2015). The carbonate content decreases down the slope of the carbonate platform, represented by marls and calcareous mudstones, and the deepest parts of the basin are formed by graptolitic shales (Hammarlund et al., 2019; Porębski et al., 2013; Sullivan et al., 2018). Deposition in such a neritic carbonate platform takes place through in situ carbonate accumulation. The closer to the onshore end of the onshore-offshore gradient, the higher the deposition rate of carbonate sediment. Therefore, we propose that carbonate content can in this setting be used to approximate the depositional rate.

1.3.3. Proportion of Pelagic Palynomorphs

Phytoplankton and zooplankton abundance in a rock sample reflects the common effect of multiple factors, including productivity, depositional rate, and taphonomy (Mullins et al., 2004). To distinguish the individual contributions of these three factors, the abundance itself would need to be transformed using an independent age model. Here we evaluate to what extent this abundance is the result of changing depositional rates by comparing the relative age model calculated from it with the two previous age models. At Bodudd, the dominant groups of organic-walled microplankton are acritarchs, prasinophytes, and chitinozoans. Of these groups, chitinozoans did not belong to phytoplankton, but they also have been reconstructed to have had an epipelagic type of distribution (Vandenbroucke et al., 2010) with only a small proportion of taxa showing association with specific facies (Bergström & Grahn, 1985; Nestor, 1998). Acritarchs, on the other hand, show strong differentiation along the onshore-offshore gradient (Mullins et al., 2004; Stricanne et al., 2004, 2006), but although the assemblages at Bodudd shift in their composition in line with increasing shallowing, the total abundance remains strongly correlated between all pelagic palynomorphs, including prasinophytes which are often observed to reach high abundance in restricted facies, for example, brackish or anoxic. Taken together, we suggest that strongly synchronous changes in the absolute abundance of all palynomorph groups regardless of their differing ecologies, as documented at Bodudd by Stricanne et al. (2006), reflect primarily their accumulation under varying depositional rates.

2. Materials and Methods

2.1. The Bodudd 1 Section, Gotland, Sweden

The strata exposed on Gotland reach from the Telychian to the Ludfordian (Calner et al., 2004a; Jeppsson et al., 2006). They represent a relatively complete sequence of Silurian sedimentary rocks, which have not undergone major burial or freshwater diagenesis (Munnecke et al., 1997; Munnecke & Samtleben, 1996). During the Silurian Period, Gotland was located near the paleoequator, on the margin of the paleocontinent of Baltica, and formed part of a large epicontinental carbonate platform. The sedimentary succession was deposited directly on a large volcanometamorphic domain of the Fennoscandian Shield, consisting of Rapakivi-type granites (Koistinen et al., 2001). The homogenous composition of this domain constrains possible variation in the composition of the influx derived from bedrock weathering.

The Ludfordian (Ludlow, upper Silurian) Bodudd 1 section is exposed along the shoreline on the SW coast of Gotland with a gentle NW dip of approximately 0.5° (Jeppsson, 2005; Figure 2). It has been logged in detail (Figure 1), and four thin sections have been produced (EJ-15-426 through EJ-15-429) to aid facies analysis (Figure 2). The northern end (57°4′15.40″N, 18°11′46.40″E) exposes strata representing the Botvide Member (När Formation, Hemse Group), which at the base is dominated by laminated marl-siltstone heterolith with pyrite concretions. The lowest 0.5 m of the section is laminated and devoid of bioturbations; above that rare *Chondrites* can be found (Bioturbation Index, BI, of 1; Taylor & Goldring, 1993). In the upper part, the carbonate and fossil contents increase and bioturbations become more common (BI 2). The younger part of the Member is a limestone-marl alternation. The fauna includes trilobites, cephalopods, brachiopods, and acanthodians, that is, a mixture of benthic and pelagic organisms. Toward the top of the När Formation at Bodudd an enrichment in dolomite, quartz sand, and silt (Samtleben et al., 2000), as well as in small cephalopods, is observed (Calner et al., 2004b). Unlike in more proximal settings, where the boundary between the Hemse Group and the Eke Formation is erosional, the transition between these units at Bodudd 1 is conformable and gradual (Calner et al., 2004b). Therefore, the boundary in this section has not been clearly defined. Hede (1921) placed it below the first appearance of oncoids, but it is not clear on which basis. Jeppsson et al. (2007) marked this boundary approximately 1.5 m below the level used here, but this placement was based on conodonts and $\delta^{13}C_{carb}$ values. Here we follow Calner et al. (2004b) in placing it at a prominent, dolomitic bed near the top of the Member. The Lower Eke Formation consists of white

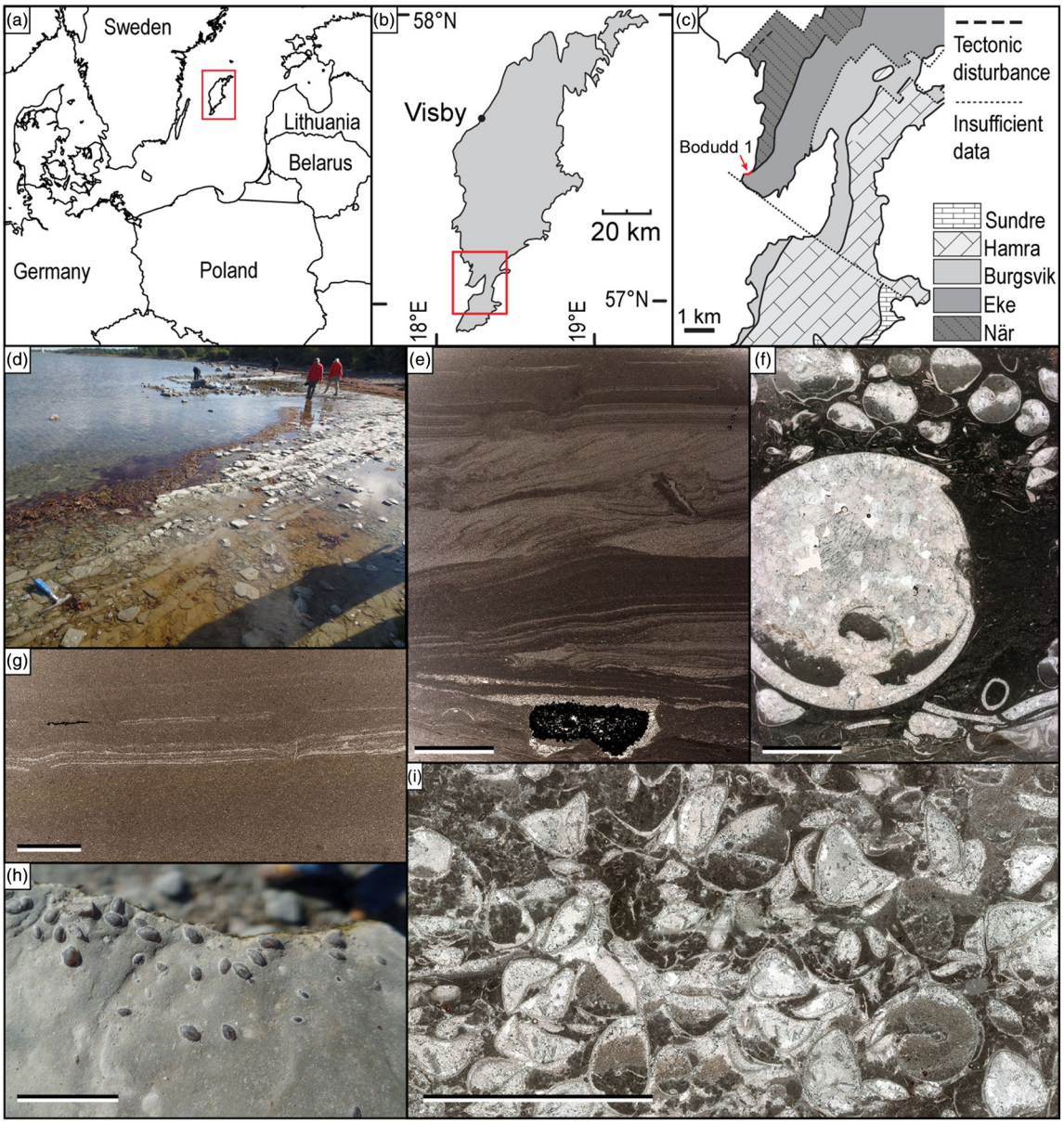

Figure 2. The Bodudd 1 section. (a–c) Location in the western coast of Gotland, Sweden; (b, c) modified from Jeppsson et al. (2007). (d) Outcrop overview. (e) Sample EJ-15-428, laminated heterolith near the base of the section. (f) Sample EJ-15-426, floatstone consisting of the brachiopod *Dayia navicula* and a cephalopod orthocone, scale bar 0.5 cm. (g) Sample EJ-15-427, silty marl, scale bar 0.3 cm. (h) Mudstone with *Dayia navicula* near the top of the När Formation, scale bar 2 cm. (i) Brachiopod-ostracod coquina in peloidal grainstone matrix, Eke Formation, scale bar 1 cm.

dolomitic mudstones with rare oncoids. Oncoids are rock-forming in the uppermost part of the section, which exposes the Middle Eke Formation. The southernmost end of the section is located at 57°4′ 12.20″N, 18°11′14.20″E.

According to the regional conodont zonation by Jeppsson (2005) and Jeppsson et al. (2006), the Botvide Member belongs to the *Polygnathoides siluricus* Zone and the Eke Formation to the icriodontid Zone, which corresponds to the lower part of the *Ozarkodina snajdri* Zone recognized in other areas (Märss & Männik, 2013). Bulk-rock carbon isotope values at Bodudd 1 have been reported to rise gradually from +1.7‰ to +6‰ in the När Formation and, over a much shorter stratigraphic thickness, to +7‰ in the Eke Formation (Jeppsson et al., 2007; Samtleben et al., 2000). These values rise further in overlying strata in nearby localities on Gotland, for example, to 7.8‰ at Bodudd 2, 8.2‰ at Ronehamn 2 (Samtleben et al., 2000), and 9.2‰ at Ronnings 1 (Jeppsson et al., 2007). The sequence-stratigraphic interpretations

based on the entire region propose a highstand systems tract and the onset of a falling stage systems tract (FSST) in the upper part of the När Formation with the FSST continuing into the lower part of the Eke Formation (Eriksson & Calner, 2008; Kozłowski & Munnecke, 2010).

Strata exposed along the shoreline at Bodudd, on the SW coast of Gotland, have been sampled at low water level in August 2014. Seventy-five samples spanning the upper part of the Hemse Group and the base of the Eke Formation have been collected for bulk-rock carbon isotope analyses. A subset of 42 samples has been used to measure rock elemental composition. The surfaces of samples have been cut off and the remainder washed, sonicated in deionized H_2O, and dried overnight at about 25°C in a cabinet desiccator. Samples used for isotope analyses only were cleaned and powdered using a hand drill. Bulk-rock isotope analyses were chosen over analyses in skeletal fossils because the lower part of the section was effectively barren and fossil sampling would not allow sufficient continuity.

2.2. Bulk-Rock Isotope Analyses

Carbon isotope analyses were performed in the Isotope Laboratory of GeoZentrum Nordbayern (Erlangen). Carbonate powders were reacted with 100% phosphoric acid at 70°C. Samples were measured using a Gasbench II connected to a ThermoFinnigan Five Plus mass spectrometer. All values are reported in per mill relative to Vienna Peedee Belemnite (V-PDB) by assigning $\delta^{13}C$ and $\delta^{18}O$ values +1.95‰ and −2.20‰ to international standard National Bureau of Standards 19 (NBS19) and −46.6‰ and −26.7‰ to international standard LSVEC, respectively. Reproducibility and accuracy were monitored by replicate analysis of laboratory standards calibrated to NBS19 and LSVEC and were better than ±0.1‰ standard deviation for both carbon and oxygen isotopes. All data are reported for calcite. The data set is available in Jarochowska et al. (2020).

2.3. Trace Element Analyses

Trace element analyses were conducted on a Thermo Scientific X-Series 2 quadrupole inductively coupled plasma mass spectrometer at GeoZentrum Nordbayern (Erlangen). For the first run of trace element analyses 15 samples mainly concentrated in the upper half of the profile were selected. These rock samples were crushed and powdered in an agate mortar. For each sample 0.1 g of rock powder was accurately weighed, and the carbonate fraction selectively dissolved using 1 M (mol/L) acetic acid following the method established by Zhao et al. (2009) to omit the contribution of the detrital fraction. Concentrations of rare earth elements (REE) have been normalized using the Post Archean Australian Shale (PAAS) according to McLennan (2001) and Piper and Bau (2013). Element concentrations were calculated from the exact weight of each powdered sample assuming that the sample is 100% carbonate. These values were then divided by the measured carbonate content of the respective sample to obtain the actual trace element concentrations. A carbonate bomb was used to determine the carbonate content in percentage by weight (wt. %) (Müller & Gastner, 1971). After analyzing the results of the first batch, a second batch of 27 samples was selected and analyzed to fill in gaps, especially in the lower half of the profile. Cerium anomaly Ce* was calculated as $[Pr] \times ([Pr] \times [Nd]^{-1})$ according to Lawrence et al. (2006). The data set is available in Jarochowska et al. (2020).

2.4. Transformation by Relative Age Models

Each of the three relative age models was created by fitting a linear regression model to the data series using ordinary least squares regression implemented in R Software (R Core Team, 2015). Figure 3 compares the obtained age models with constant deposition. Only data from the När Formation, which represented a continuous gradient of environments and depositional rate, were analyzed. Element concentrations were transformed with each of the relative age models using the `patterntodepositionmodel` function of the DAIME package for R Software (Hohmann, 2020). Ratios, that is, carbon isotope values as well as europium and cerium anomalies (Eu/Eu* and Ce/Ce*), were transformed using the `pointtransform` function, which transforms stratigraphic height to time but not the values. The results have been scaled into the original height interval of the investigated section in meters, so that the results can be directly compared with the un-transformed data (Figure 4). R codes allowing to reproduce the analysis are provided in Jarochowska et al. (2020). Figure 4 should be read as if the changes in chemical composition, as they have been transformed into the time realm, had been recorded in a sedimentary section with the same total thickness but a constant deposition rate (1:1 relationship between thickness and time).

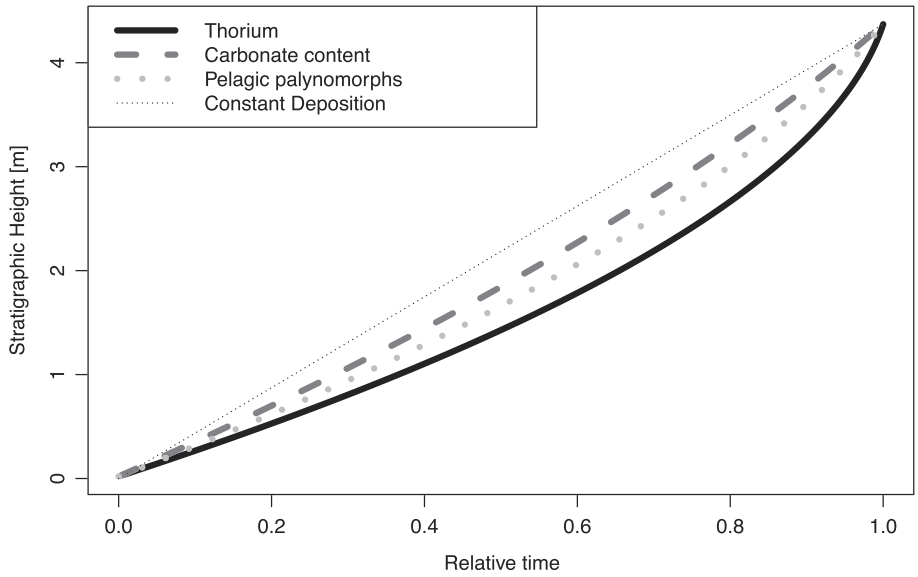

Figure 3. Relative age models calculated from three different proxies using the DAIME model.

3. Results

3.1. Bulk-Rock Carbon Isotopes

Bulk-rock $\delta^{13}C_{carb}$ values at Bodudd 1 (Figure 1 and gray lines in Figure 4) remain around 1.5‰ in the lower half of the section and start increasing at the height of 2 m to 6.1‰ at the top of the När Formation at 4.5 m. They reach 7.3‰ in the Eke Formation in the topmost part of the outcrop (5.56 m). Oxygen isotope values, used here only to screen for potential diagenetic alteration, range from −7.9‰ to −4.3‰, and the coefficient of covariation between oxygen and carbon isotope values is $R^2 = 0.3$, suggesting no major alteration (Banner & Hanson, 1990).

3.2. Trace Elements and Redox Proxies—Original Values

Vanadium and nickel concentrations (Figure 1 and gray lines in Figure 4) show high variability but overall decreasing trends in the lower part of the section (2 to 10 ppm in V, 2 to 27 ppm in Ni; Figure 1). Both elements show distinct double peaks at the stratigraphic heights of 2.38 m (7.36 ppm V, 11.56 ppm Ni; Figure 1) and 2.48 m (4.99 ppm V, 14.16 ppm Ni; Figure 1), followed by low values ranging throughout the upper part of the När Formation. Cesium concentration remains low throughout the section (mean 0.05 ppm) except for a double peak at the same levels: 0.33 and 0.14 ppm (Figure 1). This level, at which multiple elements show higher concentrations, shortly post-dates the onset of the LCIE at Bodudd 1. Uranium concentration shows different dynamics, with low levels below 2 ppm except for a single peak of 9 ppm at 0.2 m (Figure 1).

Eu/Eu* varies between 1.1 and 1.17 in the lower part of the section up to the level where V, Ni, and Cs show prominent peaks (2.38 m; Figure 1). There it has low values (1.11 and 1.10), and it remains low (1.09 to 1.12) thereafter. Ce/Ce* has mirrored dynamics, with low but variable levels in the lower part and elevated values starting with 0.93 at 2.38 m. This level of value reversal in both proxies occurs at approximately 3 m, and this point will be used further as a benchmark in comparisons between models.

3.3. Th-Based Relative Age Model

This relative age model (Figure 4a) indicates the lowest depositional rate in the lower part of the section and the most rapid increase in the upper part when comparing among all models (Figure 3). It indicates that the onset of the LCIE was even more rapid than it appears from the stratigraphic section; that is, the rise in $\delta^{13}C_{carb}$ starts at approximately 2.9 m of the section, not at 2 m as in the original data (Figure 1 and gray lines in Figure 4). Un-condensing the deeper-water deposits in the lower part of the section results in lower levels of V and Ni, as well as their lower variability: Previously noted high-frequency and high-amplitude peaks are more protracted and less dramatic; for example, the highest peak in V (10.02 ppm) has decreased by 38%

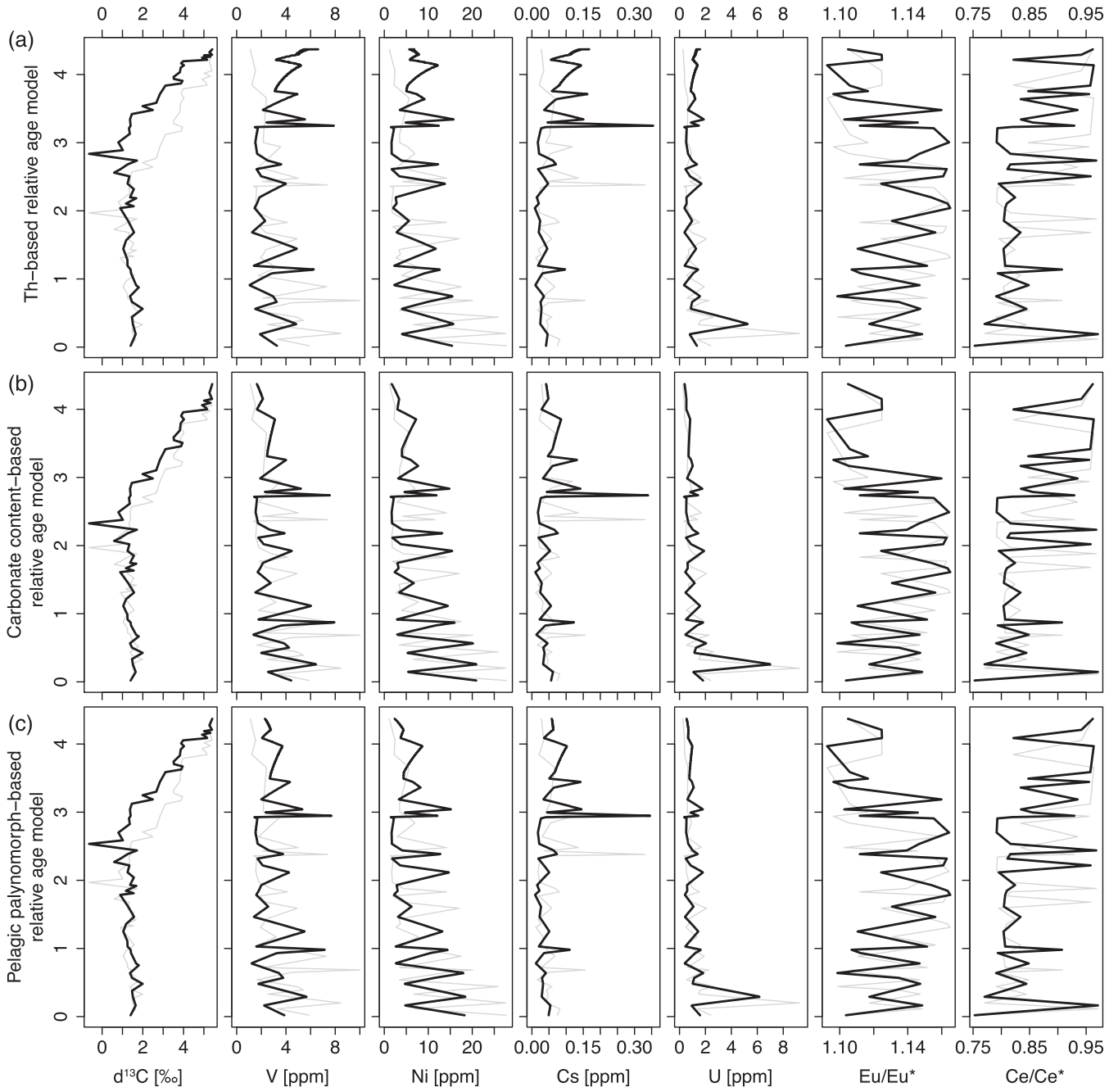

Figure 4. $\delta^{13}C_{carb}$ and redox-sensitive elemental concentrations and their ratios transformed using three relative age models (thick black lines) compared with original values (thin gray lines) in the När Formation at Bodudd 1. Eu/Eu* denotes Eu enrichment due to reduction to Eu^{2+} under reducing seawater conditions and Ce/Ce* = cerium depletion in oxygenated water owing to oxidation to Ce^{4+} and precipitation as CeO_2 (Lawrence et al., 2006; Rasmussen et al., 1998).

(6.25 ppm) in the transformed data. Similarly, the uranium peak near the base of the section decreased by 45% from 9.24 to 5.25 ppm. In other words, condensation according to this model resulted in an increase of the top absolute values by 76%. On the other hand, because the depositional rate is in this model highest in the upper part of the section, the trends in V, Ni, and Cs concentrations have been reversed from gradual decreases to step-wise increases. In the original data, V and Cs concentrations in the topmost När Formation were 1.10 and 0.03 ppm, respectively, and rose to 6.61 and 0.17 ppm after transformation. The distinct peaks identified at 2.38 and 2.48 m have, when accounting for high

depositional rate, become even higher and more abrupt, now marking the onset of rises in the concentration of their respective elements. The high depositional rate moved also the reversal of the Eu/Eu* and Ce/Ce* values from approximately 3 to 3.7 m, indicating a much shorter interval with low europium anomaly and high cerium anomaly levels.

3.4. Carbonate Content-Based Relative Age Model

The relative age model based on carbonate content deviates the least from constant deposition among the three models considered here, and, accordingly, the changes in the transformed data and their interpretation are the smallest. The onset of the LCIE is at 2.3 m instead of 2.0 m. The lower part of the section changed little under this model. V and Ni show high variability, and their concentrations have decreased less than they had in the Th-based model; for example, the peak in V decreased by 21% to 7.93 ppm. The strongest changes in the depositional rate in this model are expected in the middle part of the section, whereas the topmost part is similar to the original data; for example, there is no reversal of trends in the concentrations of V, Ni, and Cs. The U peak decreased by 25% to 6.97 ppm. The level at which Eu/Eu* and Ce/Ce* values flip has moved only approximately 0.3 m upward.

3.5. Pelagic Palynomorphs-Based Relative Age Model

In this model the onset of the LCIE is shifted upward by approximately 0.5 m. The position of peaks in the concentrations of V, Ni, and Cs above the onset of the excursion has shifted upward by approximately 0.6 m, but their reconstructed values increased only marginally: by 4% to 7.69 ppm for V, by 7% to 15.12 ppm for Ni, and by 6% to 0.35 ppm for Cs. The level at which Eu/Eu* and Ce/Ce* values reverse moved approximately 0.45 m upward. As in the model based on carbonate concentration, no increasing trend in the levels of these metals was noted in the top of the section. Also, the U peak remained sharp, and its amplitude decreased by 33%.

4. Interpretation and Discussion

4.1. The Effect of Depositional Rates

The interpretation of paleoenvironmental proxies often invokes “rapid” or “gradual” changes, even if an absolute age model is not available to gauge the tempo. This is the case, for example, for deep-time strata, where the number and the precision of geochronological dates are low, or for high-energy or redeposited strata where volcanic ash does not preserve. Often it is the relative timing of events that is of interest, for example, when biotic changes are correlated with changes in the environment (Danise et al., 2019; Pašava et al., 2017; Rita et al., 2019; Sullivan et al., 2018). Here we used a deliberately simple geological section which records a gradual facies shift from deep to shallow to illustrate how small changes in the relative depositional rates impact the paleoenvironmental proxy record. The prominent peaks in redox proxies changed their magnitudes by up to 45%, and accounting for sedimentary condensation or dilution resulted in reconstructing them as more gradual or more abrupt events. Most strikingly, in all models the carbon isotope excursion has been reconstructed as even more abrupt than it appears at face value. Similarly, coordinated double peaks in V, Ni, and Cs, as well as the reversal in europium and cerium anomalies, which all took place shortly after the onset of the excursion, were more abrupt and extended over a shorter period than it seems in Figure 1. This reflects shallowing in the upper part of the När Formation, apparent in the shift toward the interior of the carbonate platform and higher carbonate production. Based on thorium content, this rise is so rapid that concentrations of V, Ni, and Cs were effectively rising at that time, even though this rise is not discernible in the un-transformed data.

The accumulation of redox-sensitive metals in sediment is governed by three major factors: their concentration in the seawater, the dynamics (input and oxidation rate) of sedimentary organic matter, and the depositional rate (Algeo & Maynard, 2008). Here we focus on the last aspect. At high depositional rates, trace metals are diluted by sediment input and their diffusion is limited (Liu & Algeo, 2020). This effect is expected to be lower for elements enriched from the aqueous phase, for example, U, than in those which are predominately or partly enriched from the organic matter to which they are bound, such as Ni (Tribovillard et al., 2006). For elements enriched directly from water, low depositional rate allows more time for sediment enrichment, for example, of U through uranyl ion diffusion from the sediment column (Crusius & Thomson, 2000). An empirical and modeling study by Liu and Algeo (2020), which compared U and Mo

enrichment in settings with similar redox conditions but different depositional rates, confirmed that these rates exert a second-order control on the enrichment of U and Mo and can increase the enrichment by up to 400%.

Note that we refer to condensation in the way the term is used in the paleontological literature, that is, any accumulation, whether of fossils or metals, due to the slowdown of deposition (Kidwell, 1989; Kowalewski & Bambach, 2008), and not the narrower sense definition referring to condensed sediments (Föllmi, 2016). In the latter case, alteration of the concentration record by element remobilization from the sediment becomes important and would need to be taken into account.

4.2. Interpretation of Redox Proxies

Owing to the various sources and mobilities of redox proxies, redox state of the seawater is best reconstructed using a multiproxy approach. Commonly used bulk-rock concentrations represent trace metal influx present in multiple phases, not only the hydrogenous authigenic phase, but also the detrital phase which does not represent the composition of the seawater. This problem is circumvented here in that elemental concentrations were measured in the carbonate fraction only (Zhao et al., 2009). As carbonates are, at the scale of the platform, produced in situ, they are here taken to represent the conditions in the seawater at the time of their precipitation. This process includes early diagenesis, that is, lithification, precipitation of cements, and transformation of aragonite into calcite, it involves therefore a non-negligible degree of time-averaging. The caveat of this approach is that the absolute values reported here may not be directly comparable with values reported from bulk-rock analyses and that the incorporation of trace elements may be influenced by metabolic processes of carbonate-precipitating organisms.

The lowest 0.5 m at Bodudd 1 represents dysaerobic facies, which is consistent with high U concentration, although at a single level. Ni and V are also elevated at this level, but they do not co-vary with uranium and show peaks at multiple other levels. Ce/Ce* values are relatively low in this sample (0.77). Uranium enrichment is an indicator of suboxic to euxinic conditions (Algeo & Tribovillard, 2009), and it is incorporated into aragonite as well as calcite (Kelly et al., 2003; Reeder et al., 2000). However, at Bodudd 1 its lack of covariation with other proxies and occurrence in dysaerobic facies might indicate transient development of anoxic conditions at the sediment-water interface only. This would allow precipitation of U from the water at this interface, but not enrichment of organic-bound Ni and V. For Ni to become enriched in sediment, three conditions need to be met: It has to be delivered there, which happens mostly in association with organic matter, which then has to decay to release it, and sulfides need to be present (Tribovillard et al., 2006). Vanadium is also delivered to the sediment with organic matter. Its most reduced form V (III) can indicate euxinic conditions, which—however—is unlikely given the facies, but its V (IV) form can be enriched in the sediment and incorporated in calcite and aragonite (Mitchell, 2016; Smrzka et al., 2019). Both elements show strong covariation with each other as well as with cesium.

Europium and cerium anomalies show high variations throughout the section, but their mirror-like behavior can be discerned nonetheless. This variability might reflect the mixture of authigenic carbonate precipitated at the seafloor with cements precipitated within the sediment. Cerium anomaly remains at low levels, indicating depletion of the element under oxic conditions, up to approximately the onset of the LCIE at around 2 m. As $\delta^{13}C_{carb}$ values rise, Ce/Ce* also increases to levels around 0.95, suggesting suboxic conditions in the water column in this interval.

The concentrations of redox-sensitive elements and REE anomalies observed at Bodudd 1 show high variability over a short thickness of the section and over an estimated short time of deposition. This is not unexpected in shallow-water facies. The chemical composition of marine carbonates is most variable at the proximal end of the onshore-offshore transect (Coimbra et al., 2015) and cannot be compared with lithologically homogenous deep-water sections where these proxies are most commonly applied (e.g., Sullivan et al., 2018). In stark contrast with traditional approaches, where homogenous sections are analyzed to eliminate factors other than redox conditions that may affect the chemical compositions, Bodudd 1 was specifically chosen for its record of abrupt, severe changes in the relative sea level and potentially in the redox state of the water. The variability we observed is consistent between proxies, which allows us to exclude random errors as the cause for high variance. Instead, variations largely follow the dramatic facies shift associated with the rapidly falling relative sea level. The highest variability is observed in the dysoxic heterolith in

the lowest part of the section, where sedimentary structures indicate shifts between quiet settling of carbonate mud and rapid erosion by coarser material (Figure 2e). In the upper part of the section, lower variability coincides with increased bioturbation, which has likely contributed to homogenization of the values. Finally, the peak at the onset of the CIE is recorded in all proxies and even when the depositional rates are accounted for. Overall, the high variability at Bodudd 1 supports the hypothesis of a variable redox state even in shallow-water settings during the onset of the LCIE (Bowman et al., 2019; Munnecke et al., 2012; Vandenbroucke et al., 2015).

4.3. Development of Age Models

Results of transformations using the three relative age models were quantitatively different but were consistent in the direction in which they changed the interpretation. They all indicated an even faster onset of the LCIE, smaller values and lower variability of redox proxies at the base of the section, and a later position and higher amplitude of the V, Ni, and Cs peaks above this onset. These interpretations are important for the detailed reconstruction of the dynamics of this particular paleoceanographic perturbation and illustrate how the interpretation of other such events can be improved by accounting for the depositional rate. Each of the proxies used to construct relative age models is subject to other controls than the sheer onshore-offshore gradient. For instance, thorium is affected by sedimentary winnowing and focusing, by dust input (Kozłowski & Sobień, 2012), and by changes in provenance (Adams & Weaver, 1958). Major changes in provenance can be excluded here owing to the homogeneity of the underlying volcanometamorphic domain (Koistinen et al., 2001). Climate change which influences weathering and runoff also affects both thorium content and carbonate production, the latter being also sensitive to changes in seawater pH. The relative importance of these processes should be, for any section, contrasted with the sedimentary context.

In the case of Bodudd 1, the dominant change in the section is a rapid shallowing and transition from offshore, mixed siliciclastic-carbonate facies to a tropical shallow inner platform environment. This abrupt sea level fall is recorded globally (Eriksson & Calner, 2008; Kozłowski & Sobień, 2012; Loydell & Frýda, 2011; McLaughlin et al., 2019; Munnecke et al., 2010) and attributed to glacioeustasy (Sproson, 2020). Therefore, local sedimentological processes such as winnowing or changes in provenance can be excluded as driving the observed trend. The onshore-offshore gradient is the main factor differentiating multiple environmental parameters at the basin scale, including the distribution of organisms (Jarochowska et al., 2018; Scarponi & Kowalewski, 2004; Tomašových, 2006), the composition and variability of sediment composition (Coimbra et al., 2015), and Th concentration (Adams & Weaver, 1958; Doveton, 1994; Ehrenberg & Svånå, 2001). It is also manifest as the driving force behind the composition and abundance of palynomorph assemblages in the Silurian carbonate platforms (Mullins et al., 2004; Stricanne et al., 2004, 2006). The three proxies for the depositional rate used here are, therefore, a quantitative expression of directly observable and well-documented prominent facies shift. A shift from high to low primary productivity, which might have affected palynomorph concentration, has been hypothesized immediately before the onset of the LCIE (Cramer & Saltzman, 2007; Jeppsson & Aldridge, 2000). It is consistent with the overall decrease in the relative abundance of planktonic palynomorphs at Bodudd 1, if facies effect is ignored (Figure 1, Stricanne et al., 2006). However, how palynomorph abundance does or does not reflect productivity is an open question. Moreover, this decrease is associated with systematic changes in the composition, for example, an increased proportion of terrestrial spores (Stricanne et al., 2004, 2006). This shift in composition supports the alternative hypotheses by Porębska et al. (2004) and Loydell (2007) that observed changes are related to community turnover rather than changes in productivity.

Palaeoclimatic change has been associated with carbon cycle perturbations recorded during the LCIE, but its character and role are still debated. According to Jeppsson and Aldridge (2000), the times of the onset of the excursion would have been marked by a transition from humid to arid climate, which would contribute to a higher carbonate content through lower input of argillaceous material, offering a potential alternative explanation for the changes we observed. Isotopic evidence from brachiopod shells and conodont apatite supports rapid cooling during this interval (Lehnert et al., 2007; Trotter et al., 2016). Lower temperatures are expected to decrease the rates of carbonate production in the tropical factory, thus potentially weakening carbonate content as a proxy for bathymetry, but the position along the onshore-offshore gradient remains the primary control in spite of this secondary, contrasting control.

We deliberately addressed a section that is of global interest but lacks a numerical "absolute" age model to illustrate how such situation can be approached, but analogous transformations using the DAIME model can be done using numerical ages, a mixture of relative and numerical age model, and even depositional rates expressed at the ordinal scale, for example, low for transgressive and high for regressive deposits (Hohmann, 2018, 2020). The general agreement in the conclusions of the three relative models suggests that, although each of them is based on multiple assumptions, they may be sufficient for their purpose. What is more, the quantitative results of the transformation allow statistical analyses of the corrected data. Other proxies for depositional rates to base the models upon are needed for other depositional environments, so in each case a proper understanding of the depositional system is necessary; the set of proxies for depositional rates is therefore unconstrained and depends also on the depositional resolution of the given site. Concentrations of palynomorphs should, however, be applicable across various settings, including terrestrial. At the moment the models are not entirely actualistic as weathering rates and high-resolution carbonate production rates are rarely reported together with depositional rates, especially in marine settings where they are hard to measure. But the importance of this aspect for interpreting geochemical proxies is gaining appreciation (Liu & Algeo, 2020; Trayler et al., 2020). Our example includes only a small fragment of a single depositional sequence, most likely spanning just one systems tract, and therefore focuses mostly on the effect of instantaneous depositional rates. Applying the approach to sections covering longer periods would require accounting for stratigraphic completeness, that is, to estimate the positions of hiatuses and their durations (Straub et al., 2020; Tipper, 2016). Several studies have demonstrated that this is possible without absolute ages when the depositional system is well understood (Davies et al., 2019; Miall, 2015). Considering how big an impact depositional rates have on reconstructing past climate, biotic, and oceanographic changes (Kidwell, 1998; Kowalewski, 1996; Trachsel & Telford, 2017), we advocate for its imprint to be increasingly integrated in these reconstructions.

5. Conclusions

Relative age models constructed from three proxies for depositional rate have shown similar results in our Silurian text case. The model based on thorium input indicated the strongest deviation from constant depositional rate, and the model based on carbonate content the weakest. Transforming $\delta^{13}C_{carb}$, Eu/Eu*, and Ce/Ce* ratios as well as concentrations of selected redox-sensitive elements indicated that the onset of the LCIE at Bodudd appeared more protracted in terms of rock thickness than it would be under constant depositional rates. Elevated values of V, Ni, and Cs near the onset of the excursion appeared lower in the un-transformed data as a result of dilution by increased sediment input, thus allowing us to reject the hypothesis tested here that the peaks are created through sedimentary condensation; this process makes them appear more abrupt. Under the thorium-based relative age model, increasing trends in the concentrations of redox-sensitive elements appeared in the LCIE interval, whereas they were not visible in the un-transformed data. Here applied to one particular section, the general use of the DAIME model and the proxies for depositional rates can be used across the column and settings and further expanded to incorporate hiatuses and numerical ages. Our approach allows formulating testable hypotheses about stratigraphic trends in paleoenvironmental proxies, which can be further falsified or refined. This approach relies on a thorough understanding of the depositional system and the scale of measurement of the depositional rates (Miall, 2015; Tipper, 2016).

Conflict of Interest

The authors have no financial conflicts of interest.

Acknowledgments

We are grateful to Lander Soens and Jules Velleman for help with the collection of the field samples in Bodudd. We thank Ludovic Stricanne for providing sample positions for palynological data used in the study, Marcel Regelous for the ICP-MS measurements, and Wolfgang Weingut and Michael Joachimski for carbon isotope measurements. The manuscript benefited from suggestions by two anonymous reviewers.

Data Availability Statement

Data sets for this research are available in this in-text data citation reference: Jarochowska et al. (2020) (cc-By Attribution 4.0 International) (at https://osf.io/a6vwr/).

References

Adams, J. A. S., & Weaver, C. E. (1958). Thorium-to-uranium ratios as indicators of sedimentary processes: Example of concept of geochemical facies. *AAPG Bulletin*, *42*(2), 387–430.

Algeo, T. J., & Maynard, J. B. (2008). Trace-metal covariation as a guide to water-mass conditions in ancient anoxic marine environments. *Geosphere*, *4*(5), 872–887. http://geosphere.gsapubs.org/content/4/5/872.abstract, https://doi.org/10.1130/GES00174.1

Algeo, T. J., & Tribovillard, N. (2009). Environmental analysis of paleoceanographic systems based on molybdenum–uranium covariation. *Chemical Geology*, *268*(3–4), 211–225. http://www.sciencedirect.com/science/article/pii/S0009254109003805, https://doi.org/10.1016/j.chemgeo.2009.09.001

Antoshkina, A. I. (2018). The Ludfordian Lau Event (upper Silurian) in the northeastern regions of European Russia. *Stratigraphy and Geological Correlation*, *26*, 634–658. https://doi.org/10.1134/S0869593818060023

Bacon, M. P., & Anderson, R. F. (1982). Distribution of thorium isotopes between dissolved and particulate forms in the deep sea. *Journal of Geophysical Research*, *87*(C3), 2045–2056. https://doi.org/10.1029/JC087iC03p02045

Banner, J. L., & Hanson, G. N. (1990). Calculation of simultaneous isotopic and trace element variations during water-rock interaction with applications to carbonate diagenesis. *Geochimica et Cosmochimica Acta*, *54*(11), 3123–3137. https://doi.org/10.1016/0016-7037(90)90128-8

Bergström, S. M., & Grahn, Y. (1985). Biostratigraphy and paleoecology of chitinozoans in the lower Middle Ordovician of the Southern Appalachians. Paper presented at the Appalachian Basin Industrial Associates Programs.

Bowman, C. N., Young, S. A., Kaljo, D., Eriksson, M. E., Them, T. R., Hints, O., et al. (2019). Linking the progressive expansion of reducing conditions to a stepwise mass extinction event in the late Silurian oceans. *Geology*, *47*, 968–972. https://doi.org/10.1130/G46571.1

Brett, C. E. (1995). Sequence stratigraphy, biostratigraphy, and taphonomy in shallow marine environments. *PALAIOS*, *10*(6), 597–616. http://www.jstor.org/stable/3515097, https://doi.org/10.2307/3515097

Calner, M., Jeppsson, L., & Munnecke, A. (2004a). The Silurian of Gotland—Part I: Review of the stratigraphic framework, event stratigraphy, and stable carbon and oxygen isotope development. *Erlanger geologische Abhandlungen - Sonderband*, *5*, 113–131.

Calner, M., Jeppsson, L., & Munnecke, A. (2004b). The Silurian of Gotland—Part II: Guide to the IGCP 503 field meeting 2004. *Erlanger geologische Abhandlungen - Sonderband*, *5*, 133–151.

Calner, M., Kozłowska, A., Masiak, M., & Schmitz, B. (2006). A shoreline to deep basin correlation chart for the middle Silurian coupled extinction-stable isotopic event. *GFF*, *128*(2), 79–84. https://doi.org/10.1080/11035890601282079

Carroll, M., Kowalewski, M., Simões, M. G., & Goodfriend, G. A. (2016). Quantitative estimates of time-averaging in terebratulid brachiopod shell accumulations from a modern tropical shelf. *Paleobiology*, *29*, 381–402. https://www.cambridge.org/core/article/quantitative-estimates-of-timeaveraging-in-terebratulid-brachiopod-shell-accumulations-from-a-modern-tropical-shelf/43B3CE946C4BE92190C77E896E750905

Chadimová, L., Vaček, F., Sobień, K., Slavík, L., & Hladil, J. (2015). Petrophysical record of the late Silurian shallow-water carbonate facies across the Lau Event (Prague Synform, Czech Republic) and dynamic time warping alignment of the magnetic susceptibility logs. *Geological Society, London, Special Publications*, *414*, 133–155. https://sp.lyellcollection.org/content/specpubgsl/414/1/133.full.pdf, https://doi.org/10.1144/SP414.14

Coimbra, R., Immenhauser, A., Olóriz, F., Rodríguez-Galiano, V., & Chica-Olmo, M. (2015). New insights into geochemical behaviour in ancient marine carbonates (Upper Jurassic Ammonitico Rosso): Novel proxies for interpreting sea-level dynamics and palaeoceanography. *Sedimentology*, *62*, 266–302. https://doi.org/10.1111/sed.12148

Cramer, B. D., & Saltzman, M. R. (2007). Fluctuations in epeiric sea carbonate production during Silurian positive carbon isotope excursions: A review of proposed paleoceanographic models. *Palaeogeography, Palaeoclimatology, Palaeoecology*, *245*(1–2), 37–45. http://www.sciencedirect.com/science/article/pii/S0031018206003373, https://doi.org/10.1016/j.palaeo.2006.02.027

Crusius, J., & Thomson, J. (2000). Comparative behavior of authigenic Re, U, and Mo during reoxidation and subsequent long-term burial in marine sediments. *Geochimica et Cosmochimica Acta*, *64*(13), 2233–2242. http://www.sciencedirect.com/science/article/pii/S0016703799004330, https://doi.org/10.1016/S0016-7037(99)00433-0

Danise, S., Clémence, M.-E., Price, G. D., Murphy, D. P., Gómez, J. J., & Twitchett, R. J. (2019). Stratigraphic and environmental control on marine benthic community change through the early Toarcian extinction event (Iberian Range, Spain). *Palaeogeography, Palaeoclimatology, Palaeoecology*, *524*, 183–200. http://www.sciencedirect.com/science/article/pii/S0031018218309258, https://doi.org/10.1016/j.palaeo.2019.03.039

Davies, N. S., Shillito, A. P., & McMahon, W. J. (2019). Where does the time go? Assessing the chronostratigraphic fidelity of sedimentary geological outcrops in the Pliocene–Pleistocene Red Crag Formation, eastern England. *Journal of the Geological Society*, *176*, 1154–1168. https://jgs.lyellcollection.org/content/jgs/176/6/1154.full.pdf, https://doi.org/10.1144/jgs2019-056

Dominici, S., Danise, S., & Benvenuti, M. (2018). Pliocene stratigraphic paleobiology in Tuscany and the fossil record of marine megafauna. *Earth-Science Reviews*, *176*, 277–310. http://www.sciencedirect.com/science/article/pii/S0012825217302714, https://doi.org/10.1016/j.earscirev.2017.09.018

Doveton, J. H. (1994). *Geologic log interpretation* (Vol. 29). Tulsa: SEPM. https://doi.org/10.2110/scn.94.29

Ehrenberg, S. N., & Svånå, T. A. (2001). Use of spectral gamma-ray signature to interpret stratigraphic surfaces in carbonate strata: An example from the Finnmark Carbonate Platform (Carboniferous-Permian), Barents Sea. *AAPG Bulletin*, *85*(2), 295–308. https://doi.org/10.1306/8626c7c1-173b-11d7-8645000102c1865d

Emsbo, P. (2017). Sedex brine expulsions to Paleozoic basins may have changed global marine $^{87}Sr/^{86}Sr$ values, triggered anoxia, and initiated mass extinctions. *Ore Geology Reviews*, *86*, 474–486. http://www.sciencedirect.com/science/article/pii/S0169136816307594, https://doi.org/10.1016/j.oregeorev.2017.02.031

Eriksson, M. J., & Calner, M. (2008). A sequence stratigraphical model for the Late Ludfordian (Silurian) of Gotland, Sweden: implications for timing between changes in sea level, palaeoecology, and the global carbon cycle. *Facies*, *54*(2), 253–276. https://doi.org/10.1007/s10347-007-0128-y

Föllmi, K. B. (2016). Sedimentary condensation. *Earth-Science Reviews*, *152*, 143–180. http://www.sciencedirect.com/science/article/pii/S0012825215300751, https://doi.org/10.1016/j.earscirev.2015.11.016

Fürsich, F. T., & Aberhan, M. (1990). Significance of time-averaging for palaeocommunity analysis. *Lethaia*, *23*(2), 143–152. https://doi.org/10.1111/j.1502-3931.1990.tb01355.x

Gradstein, F. M., Ogg, J. G., Schmitz, M. B., & Ogg, G. M. (Eds.) (2012). *The geologic time scale 2012* (1st ed.). Amsterdam: Elsevier. Retrieved from https://ebookcentral.proquest.com

Hammarlund, E. U., Loydell, D. K., Nielsen, A. T., & Schovsbo, N. H. (2019). Early Silurian $\delta^{13}C_{org}$ excursions in the foreland basin of Baltica, both familiar and surprising. *Palaeogeography, Palaeoclimatology, Palaeoecology*, *526*, 126–135. http://www.sciencedirect.com/science/article/pii/S0031018218309519, https://doi.org/10.1016/j.palaeo.2019.03.035

Hede, J. E. (1921). *Gotlands Silurstratigrafi* (Vol. C305). Uppsala: Sveriges Geologiska Undersökning.

Hohmann, N. (2018). Quantifying the effects of changing deposition rates and hiatii on the stratigraphic distribution of fossils. (Bachelor of Science), Friedrich-Alexander-Universität Erlangen-Nürnberg, Erlangen.

Hohmann, N. (2020). DAIME: Effects of changing deposition rates (Version 2.1.1). Retrieved from https://cran.r-project.org/package=DAIME

Holland, S. M. (2000). The quality of the fossil record: A sequence stratigraphic perspective. *Paleobiology*, *26*(sp4), 148–168. https://doi.org/10.1666/0094-8373(2000)26[148:TQOTFR]2.0.CO;2

Jarochowska, E., & Kozłowski, W. (2014). Facies development and sequence stratigraphy of the Ludfordian (Upper Silurian) deposits in the Zbruch River Valley, Podolia, western Ukraine: Local facies overprint on the $\delta^{13}C_{carb}$ record of a global stable carbon isotope excursion. *Facies*, *60*, 347–369. https://doi.org/10.1007/s10347-013-0370-4

Jarochowska, E., Nohl, T., Grohganz, M., Hohmann, N., Vandenbroucke, T. R. A., & Munnecke, A. (2020). Data for "Reconstructing depositional rates and their effect on paleoenvironmental proxies: The case of the Lau Carbon Isotope Excursion in Gotland, Sweden". https://doi.org/10.17605/OSF.IO/A6VWR Retrieved from: osf.io/a6vwr

Jarochowska, E., Ray, D. C., Röstel, P., Worton, G., & Munnecke, A. (2018). Harnessing stratigraphic bias at the section scale: Conodont diversity in the Homerian (Silurian) of the Midland Platform, England. *Palaeontology*, *61*, 57–76. https://doi.org/10.1111/pala.12326

Jeppsson, L. (2005). Conodont-based revisions of the Late Ludfordian on Gotland, Sweden. *GFF*, *127*(4), 273–282. https://doi.org/10.1080/11035890501274273

Jeppsson, L., & Aldridge, R. J. (2000). Ludlow (late Silurian) oceanic episodes and events. *Journal of the Geological Society*, *157*(6), 1137–1148. https://doi.org/10.1144/jgs.157.6.1137

Jeppsson, L., Eriksson, M. E., & Calner, M. (2006). A latest Llandovery to latest Ludlow high-resolution biostratigraphy based on the Silurian of Gotland—A summary. *GFF*, *128*(2), 109–114. https://doi.org/10.1080/11035890601282109

Jeppsson, L., Talent, J. A., Mawson, R., Simpson, A. J., Andrew, A. S., Calner, M., et al. (2007). High-resolution late Silurian correlations between Gotland, Sweden, and the Broken River region, NE Australia: Lithologies, conodonts and isotopes. *Palaeogeography, Palaeoclimatology, Palaeoecology*, *245*(1–2), 115–137. http://www.sciencedirect.com/science/article/pii/S0031018206003427, https://doi.org/10.1016/j.palaeo.2006.02.032

Jerolmack, D. J., & Paola, C. (2010). Shredding of environmental signals by sediment transport. *Geophysical Research Letters*, *37*, L19401. https://doi.org/10.1029/2010GL044638

Jux, U., & Steuber, T. (1992). C_{carb}- und C_{org}-Isotopenverhältnisse in der silurischen Schichtenfolge Gotlands als Hinweise auf Meeresspiegelschwankungen und Krustenbewegungen. *Neues Jahrbuch für Geologie und Paläontologie (Abhandlungen)*, *1992*(7), 85–413. https://doi.org/10.1127/njgpm/1992/1992/385

Kelly, S. D., Newville, M. G., Cheng, L., Kemner, K. M., Sutton, S. R., Fenter, P., et al. (2003). Uranyl incorporation in natural calcite. *Environmental Science & Technology*, *37*(7), 1284–1287. https://doi.org/10.1021/es025962f

Kidwell, S. M. (1985). Palaeobiological and sedimentological implications of fossil concentrations. *Nature*, *318*(6045), 457–460. https://doi.org/10.1038/318457a0

Kidwell, S. M. (1989). Stratigraphic condensation of marine transgressive records: Origin of major shell deposits in the Miocene of Maryland. *The Journal of Geology*, *97*(1), 1–24. https://doi.org/10.1086/629278

Kidwell, S. M. (1998). Time-averaging in the marine fossil record: Overview of strategies and uncertainties. *Oceanographic Literature Review*, *45*(9), 1546–1547.

Koistinen, T., Stephens, M. B., Bogatchev, V., Nordgulen, Ø., Wennerstrøm, M., & Korhonen, J. (2001). Geological map of the Fennoscandian Shield; 1:2 million. Geological Survey of Norway.

Kowalewski, M. (1996). Time-averaging, overcompleteness, and the geological record. *The Journal of Geology*, *104*(3), 317–326. http://www.jstor.org/stable/30068194, https://doi.org/10.1086/629827

Kowalewski, M., & Bambach, R. K. (2008). The limits of paleontological resolution. In P. J. Harries (Ed.), *Approaches in high-resolution stratigraphic paleontology* (pp. 1–48). New York: Kluwer Academic/Plenum Publishers. https://doi.org/10.1007/978-1-4020-9053-0_1

Kozłowski, W., & Munnecke, A. (2010). Stable carbon isotope development and sea-level changes during the Late Ludlow (Silurian) of the Łysogóry region (Rzepin section, Holy Cross Mountains, Poland). *Facies*, *56*(4), 615–633. https://doi.org/10.1007/s10347-010-0220-6

Kozłowski, W., & Sobień, K. (2012). Mid-Ludfordian coeval carbon isotope, natural gamma ray and magnetic susceptibility excursions in the Mielnik IG-1 borehole (eastern Poland)—Dustiness as a possible link between global climate and the Silurian carbon isotope record. *Palaeogeography, Palaeoclimatology, Palaeoecology*, *339–341*, 74–97. http://www.sciencedirect.com/science/article/pii/S0031018212002283

Lawrence, M. G., Greig, A., Collerson, K. D., & Kamber, B. S. (2006). Rare earth element and yttrium variability in south east Queensland waterways. *Aquatic Geochemistry*, *12*(1), 39–72. https://doi.org/10.1007/s10498-005-4471-8

Lazauskienė, J., Šliaupa, S., Brazauskas, A., & Musteikis, P. (2003). Sequence stratigraphy of the Baltic Silurian succession: Tectonic control on the foreland infill. *Geological Society, London, Special Publications*, *208*(1), 95–115. https://sp.lyellcollection.org/content/specpubgsl/208/1/95.full.pdf, https://doi.org/10.1144/GSL.SP.2003.208.01.05

Lehnert, O., Eriksson, M. E., Calner, M., Joachimski, M., & Buggisch, W. (2007). Concurrent sedimentary and isotopic indications for global climatic cooling in the late Silurian. *Acta Palaeontologica Sinica*, *46*(suppl), 249–255.

Liu, J., & Algeo, T. J. (2020). Beyond redox: Control of trace-metal enrichment in anoxic marine facies by watermass chemistry and sedimentation rate. *Geochimica et Cosmochimica Acta*, *287*, 296–317. https://doi.org/10.1016/j.gca.2020.02.037, http://www.sciencedirect.com/science/article/pii/S0016703720301605

Loydell, D. K. (2007). Early Silurian positive $\delta^{13}C$ excursions and their relationship to glaciations, sea-level changes and extinction events. *Geological Journal*, *42*(5), 531–546. https://doi.org/10.1002/gj.1090

Loydell, D. K., & Frýda, J. (2011). At what stratigraphical level is the mid Ludfordian (Ludlow, Silurian) positive carbon isotope excursion in the type Ludlow area, Shropshire, England? *Bulletin of Geosciences*, *86*(2), 197–208. https://doi.org/10.3140/bull.geosci.1257

Märss, T., & Männik, P. (2013). Revision of Silurian vertebrate biozones and their correlation with the conodont succession. *Estonian Journal of Earth Sciences*, *62*, 181–204. https://doi.org/10.3176/earth.2013.15

McLaughlin, P. I., Emsbo, P., & Brett, C. E. (2012). Beyond black shales: The sedimentary and stable isotope records of oceanic anoxic events in a dominantly oxic basin (Silurian; Appalachian Basin, USA). *Palaeogeography, Palaeoclimatology, Palaeoecology*, *367–368*, 153–177. http://www.sciencedirect.com/science/article/pii/S0031018212005500, https://doi.org/10.1016/j.palaeo.2012.10.002

McLaughlin, P. I., Emsbo, P., Brett, C. E., Bancroft, A. M., Desrochers, A., & Vandenbroucke, T. R. A. (2019). The rise of pinnacle reefs: A step change in marine evolution triggered by perturbation of the global carbon cycle. *Earth and Planetary Science Letters*, *515*, 13–25. http://www.sciencedirect.com/science/article/pii/S0012821X19301451, https://doi.org/10.1016/j.epsl.2019.02.039

McLennan, S. M. (2001). Relationships between the trace element composition of sedimentary rocks and upper continental crust. *Geochemistry, Geophysics, Geosystems*, *2*(4), 1021. https://doi.org/10.1029/2000GC000109

Mergl, M., Frýda, J., & Kubajko, M. (2018). Response of organophosphatic brachiopods to the mid-Ludfordian (late Silurian) carbon isotope excursion and associated extinction events in the Prague Basin (Czech Republic). *Bulletin of Geosciences*, *93*, 369–400. https://doi.org/10.3140/bull.geosci.1710

Miall, A. D. (2015). Updating uniformitarianism: Stratigraphy as just a set of 'frozen accidents'. *Geological Society, London, Special Publications*, *404*, 11–36. https://sp.lyellcollection.org/content/specpubgsl/404/1/11.full.pdf, https://doi.org/10.1144/SP404.4

Mitchell, J. (2016). Precipitation of aragonite under anoxic conditions. An experimental study. (Master of Science in Geology), Mississippi State University, Mississippi.

Müller, G., & Gastner, M. (1971). The 'Karbonat-Bombe', a simple device for the determination of carbonate content in sediment, soils, and other materials. *Neues Jahrbuch für Mineralogie – Monatshefte*, *10*, 466–469.

Mullins, G. L., Aldridge, R. J., & Siveter, D. J. (2004). Microplankton associations, biofacies and palaeoenvironment of the type lower Ludlow Series, Silurian. *Review of Palaeobotany and Palynology*, *130*(1–4), 163–194. http://www.sciencedirect.com/science/article/pii/S0034666704000107, https://doi.org/10.1016/j.revpalbo.2003.12.006

Munnecke, A., Calner, M., Harper, D. A. T., & Servais, T. (2010). Ordovician and Silurian sea–water chemistry, sea level, and climate: A synopsis. *Palaeogeography, Palaeoclimatology, Palaeoecology*, *296*(3–4), 389–413. http://www.sciencedirect.com/science/article/pii/S0031018210004785, https://doi.org/10.1016/j.palaeo.2010.08.001

Munnecke, A., Delabroye, A., Servais, T., Vandenbroucke, T. R. A., & Vecoli, M. (2012). Systematic occurrences of malformed (teratological) acritarchs in the run-up of early Palaeozoic $\delta^{13}C$ isotope excursions. *Palaeogeography, Palaeoclimatology, Palaeoecology*, *367*, 137–146. http://www.sciencedirect.com/science/article/pii/S0031018212001241

Munnecke, A., & Samtleben, C. (1996). The formation of micritic limestones and the development of limestone-marl alternations in the Silurian of Gotland, Sweden. *Facies*, *34*(1), 159–176. https://doi.org/10.1007/BF02546162

Munnecke, A., Westphal, H., Reijmer, J. J., & Samtleben, C. (1997). Microspar development during early marine burial diagenesis: A comparison of Pliocene carbonates from the Bahamas with Silurian limestones from Gotland (Sweden). *Sedimentology*, *44*(6), 977–990.

Nestor, V. (1998). Chitinozoan biofacies of late early Llandovery (*Coronograptus cyphus*) age in the East Baltic. *Proceedings of the Estonian Academy of Sciences (Geology)*, *47*(4), 219–228.

Nozaki, Y., Yang, H.-S., & Yamada, M. (1987). Scavenging of thorium in the ocean. *Journal of Geophysical Research*, *92*(C1), 772–778. https://doi.org/10.1029/JC092iC01p00772

Parnell, A. C., Buck, C. E., & Doan, T. K. (2011). A review of statistical chronology models for high-resolution, proxy-based Holocene palaeoenvironmental reconstruction. *Quaternary Science Reviews*, *30*(21–22), 2948–2960. http://www.sciencedirect.com/science/article/pii/S0277379111002356, https://doi.org/10.1016/j.quascirev.2011.07.024

Pašava, J., Frýda, J., & Štorch, P. (2017). Trace element variations as a proxy for reconstruction of palaeoenvironmental changes during the late Aeronian faunal and carbon isotope perturbations: New data from the peri-Gondwanan region. *Geological Quarterly*, *61*, 91–98. Aeronian, graptolite mass extinction, redox-sensitive trace elements, Barrandian area, Bohemian Massif. https://gq.pgi.gov.pl/article/view/25511

Piper, D. Z., & Bau, M. (2013). Normalized rare earth elements in water, sediments, and wine: Identifying sources and environmental redox conditions. *American Journal of Analytical Chemistry*, *4*(10), 69–83. https://doi.org/10.4236/ajac.2013.410a1009, https://www.scirp.org/journal/paperinformation.aspx?paperid=38577

Porębska, E., Kozłowska-Dawidziuk, A., & Masiak, M. (2004). The *lundgreni* event in the Silurian of the east European platform, Poland. *Palaeogeography, Palaeoclimatology, Palaeoecology*, *213*(3–4), 271–294. https://doi.org/10.1016/j.palaeo.2004.07.013

Porębski, S. J., Prugar, W., & Zacharski, J. (2013). Silurian shales of the east European platform in Poland—Some exploration problems. *Geological Review*, *61*, 630–638.

Radkovets, N. (2015). The Silurian of southwestern margin of the east European platform (Ukraine, Moldova and Romania): Lithofacies and palaeoenvironments. *Geological Quarterly*, *59*, 105–118. East European Platform, Silurian, lithofacies, reef, shelf of Baltica, palaeoenvironments. https://gq.pgi.gov.pl/article/view/13844

Rasmussen, B., Buick, R., & Taylor, W. R. (1998). Removal of oceanic REE by authigenic precipitation of phosphatic minerals. *Earth and Planetary Science Letters*, *164*(1–2), 135–149. http://www.sciencedirect.com/science/article/pii/S0012821X9800199X, https://doi.org/10.1016/S0012-821X(98)00199-X

Ray, D. C., & Thomas, A. T. (2007). Carbonate depositional environments, sequence stratigraphy and exceptional skeletal preservation in the much Wenlock limestone formation (Silurian) of Dudley, England. *Palaeontology*, *50*(1), 197–222. https://doi.org/10.1111/j.1475-4983.2006.00607.x

Reeder, R. J., Nugent, M., Lamble, G. M., Tait, C. D., & Morris, D. E. (2000). Uranyl incorporation into calcite and aragonite: XAFS and luminescence studies. *Environmental Science & Technology*, *34*(4), 638–644. https://doi.org/10.1021/es990981j

Ridgwell, A. (2005). A mid Mesozoic revolution in the regulation of ocean chemistry. *Marine Geology*, *217*(3–4), 339–357. http://www.sciencedirect.com/science/article/pii/S0025322705000575, https://doi.org/10.1016/j.margeo.2004.10.036

Rita, P., Nätscher, P., Duarte, L. V., Weis, R., & Baets, K. D. (2019). Mechanisms and drivers of belemnite body-size dynamics across the Pliensbachian-Toarcian crisis. *Royal Society Open Science*, *6*, 190494. https://doi.org/10.1098/rsos.190494

Robinson, L. F., Belshaw, N. S., & Henderson, G. M. (2004). U and Th concentrations and isotope ratios in modern carbonates and waters from the Bahamas. *Geochimica et Cosmochimica Acta*, *68*(8), 1777–1789. http://www.sciencedirect.com/science/article/pii/S0016703703007361, https://doi.org/10.1016/j.gca.2003.10.005

R Core Team (2015). *R: A language and environment for statistical computing*. Vienna: R Foundation for Statistical Computing. Retrieved from. https://www.r-project.org/

Samtleben, C., Munnecke, A., & Bickert, T. (2000). Development of facies and C/O-isotopes in transects through the Ludlow of Gotland: Evidence for global and local influences on a shallow-marine environment. *Facies*, *43*(1), 1–38. https://doi.org/10.1007/BF02536983

Samtleben, C., Munnecke, A., Bickert, T., & Pätzold, J. (1996). The Silurian of Gotland (Sweden): Facies interpretation based on stable isotopes in brachiopod shells. *Geologische Rundschau*, *85*(2), 278–292. https://doi.org/10.1007/BF02422234

Scarponi, D., & Kowalewski, M. (2004). Stratigraphic paleoecology: Bathymetric signatures and sequence overprint of mollusk associations from upper Quaternary sequences of the Po Plain, Italy. *Geology*, *32*(11), 989–992. https://doi.org/10.1130/G20808.1

Schlager, W. (2003). Sedimentation rates and growth potential of tropical, cool-water and mud-mound carbonate systems. *Geological Society, London, Special Publications*, *178*(1), 217–227. https://doi.org/10.1144/gsl.sp.2000.178.01.14

Shen, C.-C., Li, K.-S., Sieh, K., Natawidjaja, D., Cheng, H., Wang, X., et al. (2008). Variation of initial $^{230}Th/^{232}Th$ and limits of high precision U–Th dating of shallow-water corals. *Geochimica et Cosmochimica Acta*, *72*(17), 4201–4223. http://www.sciencedirect.com/science/article/pii/S0016703708003736, https://doi.org/10.1016/j.gca.2008.06.011

Smolarek, J., Trela, W., Bond, D. P. G., & Marynowski, L. (2016). Lower Wenlock black shales in the northern Holy Cross Mountains, Poland: Sedimentary and geochemical controls on the Ireviken event in a deep marine setting. *Geological Magazine*, *154*, 247–264. https://www.cambridge.org/core/article/lower-wenlock-black-shales-in-the-northern-holy-cross-mountains-poland-sedimentary-and-geochemical-controls-on-the-ireviken-event-in-a-deep-marine-setting/F12E14EB73896AE55BA97FDFFE1FED58

Smrzka, D., Zwicker, J., Bach, W., Feng, D., Himmler, T., Chen, D., & Peckmann, J. (2019). The behavior of trace elements in seawater, sedimentary pore water, and their incorporation into carbonate minerals: A review. *Facies*, *65*, 41. https://doi.org/10.1007/s10347-019-0581-4

Sproson, A. D. (2020). Pacing of the latest Ordovician and Silurian carbon cycle by a ~4.5 Myr orbital cycle. *Palaeogeography, Palaeoclimatology, Palaeoecology*, *540*, 109543. https://doi.org/10.1016/j.palaeo.2019.109543

Straub, K. M., Duller, R. A., Foreman, B. Z., & Hajek, E. A. (2020). Buffered, incomplete, and shredded: The challenges of reading an imperfect stratigraphic record. *Journal of Geophysical Research: Earth Surface*, *125*, e2019JF005079. https://doi.org/10.1029/2019JF005079

Stricanne, L., Munnecke, A., & Pross, J. (2006). Assessing mechanisms of environmental change: Palynological signals across the Late Ludlow (Silurian) positive isotope excursion ($\delta^{13}C$, $\delta^{18}O$) on Gotland, Sweden. *Palaeogeography, Palaeoclimatology, Palaeoecology*, *230*(1–2), 1–31. http://www.sciencedirect.com/science/article/pii/S0031018205004050, https://doi.org/10.1016/j.palaeo.2005.07.003

Stricanne, L., Munnecke, A., Pross, J., & Servais, T. (2004). Acritarch distribution along an inshore–offshore transect in the Gorstian (lower Ludlow) of Gotland, Sweden. *Review of Palaeobotany and Palynology*, *130*(1–4), 195–216. http://www.sciencedirect.com/science/article/pii/S0034666704000119, https://doi.org/10.1016/j.revpalbo.2003.12.007

Sullivan, N. B., Loydell, D. K., Montgomery, P., Molyneux, S. G., Zalasiewicz, J., Ratcliffe, K. T., et al. (2018). A record of late Ordovician to Silurian oceanographic events on the margin of Baltica based on new carbon isotope data, elemental geochemistry, and biostratigraphy from two boreholes in central Poland. *Palaeogeography, Palaeoclimatology, Palaeoecology*, *490*, 95–106. http://www.sciencedirect.com/science/article/pii/S0031018217305977, https://doi.org/10.1016/j.palaeo.2017.10.016

Taylor, A. M., & Goldring, R. (1993). Description and analysis of bioturbation and ichnofabric. *Journal of the Geological Society*, *150*(1), 141–148. https://jgs.lyellcollection.org/content/jgs/150/1/141.full.pdf, https://doi.org/10.1144/gsjgs.150.1.0141

Tipper, J. C. (2016). Measured rates of sedimentation: What exactly are we estimating, and why? *Sedimentary Geology*, *339*, 151–171. http://www.sciencedirect.com/science/article/pii/S003707381630029X, https://doi.org/10.1016/j.sedgeo.2016.04.003

Tomašových, A. (2006). Brachiopod and bivalve ecology in the Late Triassic (Alps, Austria): Onshore-offshore replacements caused by variations in sediment and nutrient supply. *PALAIOS*, *21*(4), 344–368. https://doi.org/10.2110/palo.2005.P05-53e

Tomašových, A., Gallmetzer, I., Haselmair, A., Kaufman, D. S., Vidović, J., & Zuschin, M. (2017). Stratigraphic unmixing reveals repeated hypoxia events over the past 500 yr in the northern Adriatic Sea. *Geology*, *45*, 363–366. https://doi.org/10.1130/G38676.1

Tomašových, A., & Kidwell, S. M. (2010). Predicting the effects of increasing temporal scale on species composition, diversity, and rank-abundance distributions. *Paleobiology*, *36*(4), 672–695. https://doi.org/10.1666/08092.1

Tomczykowa, E. (1988). Silurian and lower Devonian biostratigraphy and Palaeoecology in Poland. *Biuletyn Instytutu Geologicznego*, *359*, 21–41.

Trachsel, M., & Telford, R. J. (2017). All age–depth models are wrong, but are getting better. *The Holocene*, *27*, 860–869. https://doi.org/10.1177/0959683616675939

Trayler, R. B., Schmitz, M. D., Cuitiño, J. I., Kohn, M. J., Bargo, M. S., Kay, R. F., et al. (2020). An improved approach to age-modeling in deep time: Implications for the Santa Cruz formation, Argentina. *GSA Bulletin*, *132*, 233–244. https://doi.org/10.1130/B35203.1

Tribovillard, N., Algeo, T. J., Lyons, T., & Riboulleau, A. (2006). Trace metals as paleoredox and paleoproductivity proxies: An update. *Chemical Geology*, *232*(1–2), 12–32. http://www.sciencedirect.com/science/article/pii/S000925410600132X, https://doi.org/10.1016/j.chemgeo.2006.02.012

Trotter, J. A., Williams, I. S., Barnes, C. R., Männik, P., & Simpson, A. (2016). New conodont $\delta^{18}O$ records of Silurian climate change: Implications for environmental and biological events. *Palaeogeography, Palaeoclimatology, Palaeoecology*, *443*, 34–48. https://doi.org/10.1016/j.palaeo.2015.11.011

Vandenbroucke, T. R. A., Armstrong, H. A., Williams, M., Paris, F., Sabbe, K., Zalasiewicz, J. A., et al. (2010). Epipelagic chitinozoan biotopes map a steep latitudinal temperature gradient for earliest late Ordovician seas: Implications for a cooling late Ordovician climate. *Palaeogeography, Palaeoclimatology, Palaeoecology*, *294*(3–4), 202–219. http://www.sciencedirect.com/science/article/pii/S0031018209005215, https://doi.org/10.1016/j.palaeo.2009.11.026

Vandenbroucke, T. R. A., Emsbo, P., Munnecke, A., Nuns, N., Duponchel, L., Lepot, K., et al. (2015). Metal-induced malformations in early Palaeozoic plankton are harbingers of mass extinction. *Nature Communications*, *6*, 7966. https://doi.org/10.1038/ncomms8966

Vandenbroucke, T. R. A., Munnecke, A., Leng, M. J., Bickert, T., Hints, O., Gelsthorpe, D., et al. (2013). Reconstructing the environmental conditions around the Silurian Ireviken event using the carbon isotope composition of bulk and palynomorph organic matter. *Geochemistry, Geophysics, Geosystems*, *14*, 86–101. https://doi.org/10.1029/2012GC004348

Vecoli, M., Riboulleau, A., & Versteegh, G. J. M. (2009). Palynology, organic geochemistry and carbon isotope analysis of a latest Ordovician through Silurian clastic succession from borehole Tt1, Ghadamis Basin, southern Tunisia, North Africa: Palaeoenvironmental interpretation. *Palaeogeography, Palaeoclimatology, Palaeoecology*, *273*(3–4), 378–394. http://www.sciencedirect.com/science/article/pii/S0031018208003441, https://doi.org/10.1016/j.palaeo.2008.05.015

Wenzel, B., & Joachimski, M. M. (1996). Carbon and oxygen isotopic composition of Silurian brachiopods (Gotland/Sweden): Palaeoceanographic implications. *Palaeogeography, Palaeoclimatology, Palaeoecology*, *122*(1–4), 143–166. http://www.sciencedirect.com/science/article/pii/0031018295000941, https://doi.org/10.1016/0031-0182(95)00094-1

Wigforss-Lange, J. (1999). Carbon isotope ^{13}C enrichment in upper Silurian (Whitcliffian) marine calcareous rocks in Scania, Sweden. *GFF*, *121*(4), 273–279. https://doi.org/10.1080/11035899901214273

Young, S. A., Benayoun, E., Kozik, N. P., Hints, O., Martma, T., Bergström, S. M., & Owens, J. D. (2020). Marine redox variability from Baltica during extinction events in the latest Ordovician–early Silurian. *Palaeogeography, Palaeoclimatology, Palaeoecology*, *554*, 109792. http://www.sciencedirect.com/science/article/pii/S0031018220302376

Zhao, Y.-Y., Zheng, Y.-F., & Chen, F. (2009). Trace element and strontium isotope constraints on sedimentary environment of Ediacaran carbonates in southern Anhui, South China. *Chemical Geology*, *265*(3–4), 345–362. http://www.sciencedirect.com/science/article/pii/S0009254109002058, https://doi.org/10.1016/j.chemgeo.2009.04.015